Journal of Chemical Neuroanatomy 61–62 (2014) 176–188

Contents lists available at ScienceDirect

Journal of Chemical Neuroanatomy

journal homepage: www.elsevier.com/locate/jchemneu

Visuospatial learning and memory in the *Cebus apella* and microglial morphology in the molecular layer of the dentate gyrus and CA1 lacunosum molecular layer

Carlos Santos-Filho [a], Camila M. de Lima [a], César A.R. Fôro [a], Marcus A. de Oliveira [a], Nara G.M. Magalhães [a], Cristovam Guerreiro-Diniz [a], Daniel G. Diniz [a], Pedro F. da C. Vasconcelos [b], Cristovam W.P. Diniz [a,*]

[a] *Laboratório de Investigações em Neurodegeneração e Infecção, Hospital Universitário João de Barros Barreto, Instituto de Ciências Biológicas, Universidade Federal do Pará, Belém, Pará, Brazil*
[b] *Instituto Evandro Chagas, IEC, Ananindeua, Pará, Brazil*

ARTICLE INFO

Article history:
Received 11 July 2014
Received in revised form 18 September 2014
Accepted 13 October 2014
Available online 22 October 2014

Keywords:
Paired associates learning
Spatial memory
Microglial morphology
Dentate gyrus
Cebus apella

ABSTRACT

We investigated whether the morphology of microglia in the molecular layer of the dentate gyrus (DG-Mol) or in the lacunosum molecular layer of CA1 (CA1-LMol) was correlated with spatial learning and memory in the capuchin monkey (*Cebus apella*). Learning and memory was tested in 4 monkeys with visuo-spatial, paired associated learning (PAL) tasks from the Cambridge battery of neuropsychological tests. After testing, monkeys were sacrificed, and hippocampi were sectioned. We specifically immunolabeled microglia with an antibody against the adapter binding, ionized calcium protein. Microglia were selected from the middle and outer thirds of the DG-Mol ($n = 268$) and the CA1-LMol ($n = 185$) for three-dimensional reconstructions created with Neurolucida and Neuroexplorer software. Cluster and discriminant analyses, based on microglial morphometric parameters, identified two major morphological microglia phenotypes (types I and II) found in both the CA1-LMol and DG-Mol of all individuals. Compared to type II, type I microglia were significantly smaller, thinner, more tortuous and ramified, and less complex (lower fractal dimensions). PAL performance was both linearly and non-linearly correlated with type I microglial morphological features from the rostral and caudal DG-Mol, but not with microglia from the CA1-LMol. These differences in microglial morphology and correlations with PAL performance were consistent with previous proposals of hippocampal regional contributions for spatial learning and memory. Our results suggested that at least two morphological microglial phenotypes provided distinct physiological roles to learning-associated activity in the rostral and caudal DG-Mol of the monkey brain.

Introduction

Recent reports showed that the dynamics of microglial processes are regulated by sensory experience and neuronal activity (Wake et al., 2009; Tremblay et al., 2010). Indeed, Parkhurst et al. (2013) compared microglial-depleted and control mice and found that microglia seemed to be essential for a series of behavioral tasks, including novel object recognition; moreover, the learning-induced formation of glutamatergic synapses was mediated by a microglial-derived, neurotrophic factor (BDNF). In addition, when adult rats were trained to remember the spatial location of an object, synapse remodeling was evident six hours later, in the molecular layer of the dorsal dentate gyrus (DG-Mol) (Scully et al., 2012), and that remodeling was a microglia dependent event (Lim et al., 2013; Zabel and Kirsch, 2013). Thus, microglia-dependent remodeling seems to be a morphological expression of spatial learning consolidation (Scully et al., 2012).

Taken together, those results raised important questions related to microglial cells and cognition. For example, could microglial cell morphology in the hippocampus and dentate gyrus be correlated with performance in object identity tasks and spatial learning and memory tests? Based on observations that synaptic morphological changes seemed to be higher in the target layers of the entorhinal-to-dentate gyrus projections (Scully et al., 2012),

* Corresponding author. Tel.: +0055 91 32016756; fax: +0055 91 32016756.
E-mail address: cwpdiniz@gmail.com (Cristovam W.P. Diniz).

http://dx.doi.org/10.1016/j.jchemneu.2014.10.001
0891-0618/

and that synaptic remodeling was microglia-dependent (Kettenmann et al., 2013; Wake et al., 2013; Zabel and Kirsch, 2013; Gomez-Nicola and Perry, 2014), we hypothesized that significant microglial morphological changes may be apparent in the DG-Mol layer after spatial learning memory consolidation. Typically, microglia have been classified into two main morphological types: the first is a ramified morphology, found in microglia in the homeostatic healthy brain; the second is an amoeboid morphology, representative of activated microglia found at sites of brain injury. However, these morphologies are only extreme examples of a dynamic process; microglial morphology may change in association with neuroprotective, proinflammatory, cytotoxic, immunoregulatory, and repair functions (Hanisch and Kettenmann, 2007; Benarroch, 2013; Miyamoto et al., 2013; Gomez-Nicola and Perry, 2014). Therefore, it is necessary to quantify the subtleties of microglial morphology to gain insight into functional variability (Karperien et al., 2013).

In the present report, we investigated the morphological variability of microglia in the external and middle thirds of the DG-Mol and in the lacunosum molecular layer of CA1 (Guerreiro-Diniz et al., 2010), and analyzed correlations between morphology and results from the paired associates learning and memory (PAL) test, in *Cebus apella*, a New World monkey with remarkable cognitive capacities (Tavares and Tomaz, 2002; Resende et al., 2003; Dufour et al., 2006; VanMarle et al., 2006; Spinozzi et al., 2007). We used the PAL test from the Cambridge neuropsychological test battery (CANTAB), previously used in both human (Facal et al., 2009; Skolimowska et al., 2011) and nonhuman primates (Spinelli et al., 2004; Nagahara et al., 2010; Rodriguez et al., 2011). We measured microglial morphometric features from the external and middle thirds of the DG-Mol layers and from the lacunosum molecular layer of CA1, and subjected them to cluster and discriminant analysis. The morphological variables that contributed to cluster formation were analyzed for correlations to PAL performance.

Methods

Due to ethical considerations, the use of *Cebus apella* is sparing, and results are very valuable (Lynch Alfaro et al., 2014). Therefore, we optimized the study design to use the tissue as efficiently as possible. Four sexually immature *Cebus apella* (Wirz and Riviello, 2008), 3 ± 0.57 years old, 2 females (*S* and *M*, two years old) and 2 males (*F* and *J*, 4 years olds), were donated by the Brazilian Institute of the Environment (IBAMA), a federal institution that regulates the use of wild animals in scientific research. These animals had been previously used in other behavioral studies to measure object recognition. The animals remained in an enriched animal house, under 12-h natural daylight cycles, with food and water ad libitum, until the day of euthanasia. All procedures were carried out under the approval of the Institutional Ethics Committee for Animal Experimentation of the Federal University of Para, in accordance with NIH and Brazilian regulations for scientific procedures on animals. All efforts were made to minimize the number and suffering of the animals.

Behavioral modeling and analysis

All subjects were assessed individually. A touch screen monitor (Monitor Touch LCD, color, 17 inches, Elo/Tyco 1715L, Elo Touch Systems) was used to present all visuospatial stimuli for PAL testing. The monitor was controlled with CANTAB battery software (Cambridge Cognition, Cambridge, UK) run on a computer. An automated reward food dispenser (Med Associates Inc., USA) delivered food for correct answers; this system was used to maintain motivation throughout all sessions. Because *Cebus apella* naturally explore new environments and objects, it was relatively easy to motivate individuals to explore a marble training box (50 × 50 × 50 cm), which contained the touch screen monitor on one wall. This training box was placed at the end of a short tunnel that linked individual cages to the apparatus; this design was used to avoid contact between monkeys and the investigator and to reduce stress during the training period. All tests were recorded with a webcam. Progressive modeling procedures were adopted to ensure that, at the end of the study period, only correct answers were rewarded. We started with a motor screening task (MOT) that introduced the CANTAB touchscreen to the subjects. MOT provides a general assay that tests whether sensorimotor or other difficulties limit collecting valid data from each subject. Each animal was modeled throughout three different stages. In the first stage, when the animal paid attention to the stimuli on the screen, a reward was delivered; in the second stage, the animal was required to pay attention and touch the visual stimulus, independent of pressure on the screen, to receive a reward; and in the third stage, the animal was required to touch the stimuli with precision and adequate pressure to receive a reward. After 28 days, all animals were well adapted to the touch screen system, and they were moved to the reversion rule test. This test intended to train subjects to follow and reverse a rule. First, subjects must touch the smaller of two displayed circles; then, after 20 trials, subjects must touch the larger circle for 20 more trials. Although animals had different learning rates, after 90 days, all subjects had completed this task, and were moved to the PAL test. In the PAL test, six boxes are displayed on the screen, and they are opened in a randomized order to show the contents. One of the boxes will contain a pattern. The pattern inside is then displayed in the middle of the screen, and the subjects must touch the box where the pattern was originally located. If the subject makes an error, the patterns are re-presented to remind the subject of their locations. Each subject is given 10 trials to touch the correct box. After 10 trials, if no correct answer is obtained, the test is terminated. In the present work, only the first two steps of the first stage of the PAL test were completed successfully by all subjects. This stage required the subjects to recognize the spatial location of only one object.

Perfusion, histology, and immunohistochemistry

Animals were euthanized with an overdose of a mixture of xylazine (10 mg/kg) and ketamine (100 mg/kg). Then, brain tissues were perfused through the cardiovascular system with heparinized saline, followed by aldehyde fixative (4% paraformaldehyde, 0.1 M phosphate buffer, pH 7.2–7.4). The complete hippocampus and dentate gyrus were removed, and then, a vibratome was used to section the tissues in the coronal plane to generate 10 series of 100-μm thick sections. One series of sections (1:10) was immunolabeled with a polyclonal antibody against ionized calcium binding adapter molecule 1 (anti-IBA1, #019-19741; Wako Pure Chemical Industries Ltd., Osaka, Japan), which could detect microglia and/or macrophages. For immunolabeling, sections were pre-treated by free-floating them in 0.2 M boric acid (pH 9) at 65–70 °C for 60 min to improve antigen retrieval. Next, sections were washed in 5% Triton in PBS, and incubated in methanol with 3% H2O2. Sections were then immersed for 20 min in 10% normal horse serum, and transferred to the primary antibody solution for three days in the refrigerator (4–8 °C) with gentle, continuous agitation. Washed sections were then incubated overnight in the secondary antibody (horse anti-mouse, 1:200 in PBS), followed by immersion in ABC solution (1:100 in 0.1 M PO4 buffer pH 7.2–7.4), for 60 min as recommended by the suppliers (Vector Laboratories, Burlingame, CA, USA). Sections were then washed and visualized by reacting with horseradish peroxidase (HRP), enhanced with the glucoseoxidase-DAB-nickel method (Shu et al., 1988). All reacted sections were mounted on glass slides coated with an aqueous solution of gelatin (4.5%) and chromium potassium sulfate 4.0%. The slides were air-dried at room temperature, dehydrated, and cleared in an alcohol and xylene series. The brains of all subjects were processed for immunohistochemistry with the same procedures, and all three-dimensional (3-D) reconstructions were performed with the same equipment and software. The specificity of the immunohistochemical pattern was confirmed in control slides, treated identically, but without primary antibody (Saper and Sawchenko, 2003). These negative controls displayed no immunolabeling in any structures.

Microglial Cell 3-D reconstruction and quantitative morphology

To analyze brain sections, we used a NIKON Eclipse 80i microscope (Nikon, Japan), equipped with a motorized stage (MAC6000, Ludl Electronic Products, Hawthorne, NY, USA). Microglia from different regions of interest were analyzed under oil immersion, with a high-resolution, 100 × oil immersion, plan fluoride objective (Nikon, NA 1.3, DF = 0.19 μm). Images were acquired with Neurolucida software (MBF Bioscience Inc., Frederick, MD, USA). Although shrinkage in the *z*-axis is not a linear event, the software used in the present study corrected the shrinkage in the *z*-axis, based on previous evidence of 75% shrinkage (Carlo and Stevens, 2011). Without correction, this shrinkage would significantly distort the length measurements along this axis. Only cells with dendritic trees that were unequivocally complete were included for 3D analysis (cells were discarded when dendrite branches appeared artificially cut or not fully immunolabeled). Terminal branches were typically thin. Although many morphological features were analyzed, here, we described only those that were significantly different between subjects. We estimated and compared 22 microglial morphological parameters; 10 related to the soma and 12 to the microglial branches, as follows: (1) branch length (μm); (2) total tree length (μm) (3) surface area (μm^2); (4) branch volume (μm^3); (5) segments/mm; (6) tortuosity; (7) fractal dimensions (*k*-dim); (8) base diameter of the primary branch (μm); (9) total number of segments; (10) number of varicosities; (11) planar angle; (12) number of trees; (13) soma area (μm^2); (14) soma perimeter; (15) ferret minimum diameter; (16) ferret maximum diameter (maximum diameter in a shape); (17) compactness; (18) form factor; (19) solidity; (20) roundness; (21) aspect ratio; and (22) convexity. Thus, all microglia of each area or lamina of interest were measured multiple times, and dedicated software (Neuroexplorer, MicroBright Field Inc.) was used to process data obtained with Neurolucida. These morphological parameters (defined in Table 1) were used to investigate possible features shared by the microglia found in the regions and layers of interest. For detailed information and definitions please see: http://mbfbioscience.com/technical-support-center.

Table 1
Definitions of the morphological parameters used to quantify and compare dentate gyrus and CA1 microglial features in the *Cebus apella*.

Branched structure analysis	
Segment	Any portion of microglial branched structure with endings that are either nodes or terminations with no intermediate nodes
Segment length	Total length of the traced segment
Segments (mm0	Number of segments/total length of the segments expressed in millimeters
Branch length	Total length of the line segments used to trace the branch of interest
Total tree length	Total length for all branches in the tree mean = [length]/[number of branches]
Tortuosity	= [Actual length of the segment]/[distance between the endpoints of the segment]. The smallest value is 1; this represents a straight segment. Tortuosity allows segments of different lengths to be compared in terms of the complexity of the paths they take
Surface area	Computed by modeling each branch as a frustum (truncated right circular cone)
Branch volume	Computed by modeling each piece of each branch as a frustum
Base diameter of primary branch	Diameter at the start of the 1st segment
Planar angle	Computed based on the endpoints of the segments. It refers to the change in direction of a segment relative to the previous segment
K-dim	The "k-dim" of the fractal analysis, describes how the structure of interest fills space. Significant statistical differences in K-dim suggest morphological dissimilarities
No of varicosities, segments, trees	Refer to the total number of varicosities, segments and trees found in a single microglial cell
Cell body	
Area	Refers to the 2-dimensional cross-sectional area contained within the boundary of the cell body
Perimeter	Length of the contour representing the cell body
Feret max/min	Largest and smallest dimensions of the cell body as if a caliper was used to measure across the contour. The two measurements are independent of one another and not necessarily at right angles to each other
Aspect ratio	Aspect ratio = [min diameter]/[max diameter] indicates the degree of flatness of the cell body: •range of values is 0–1 •a circle has an aspect ratio of 1
Compactness	Compactness $= (\sqrt{(4/\pi)} \times \text{area})/\text{max diam}$ •the range of values is 0 to 1 •a circle is the most compact shape (compactness = 1)
Convexity	Convexity = [convex perimeter]/[perimeter] •a completely convex object does not have indentations, and has a convexity value of 1 (e.g., circles, ellipses, and squares) •concave objects have convexity values less than 1 •contours with low convexity have a large boundary between inside and outside areas
Form factor	Form factor $= 4\pi \times \left(\text{area}/\text{perimeter}^2\right)$ •As the contour shape approaches that of a perfect circle, this value approaches a maximum of 1.0 •As the contour shape flattens out, this value approaches 0
Roundness	Roundness = $[\text{compactness}]^2$ use to differentiate objects that have small compactness values
Solidity	Solidity = [area]/[convex area] the area enclosed by a 'rubber band' stretched around a contour is called the convex area •circles, squares, and ellipses have a solidity of 1 •indentations in the contour take area away from the convex area, decreasing the actual area within the contour

Photomicrography

For photomicrographs, we used a digital camera (Axiocan - HRC, Zeiss, Gottingen, Germany), coupled to a NIKON Eclipse 80i microscope. Digital photomicrographs were processed with Adobe Photoshop software; scaling and adjustments to the brightness and contrast were applied to the whole image. To illustrate the different microglia types, we selected 3-D reconstructions of microglia with morphometric values closest to the mean of the corresponding morphological features for each individual type in each target area and layer of interest.

Statistical analysis

Paired associates learning test—PAL

We estimated the learning index of each subject as a function of the number of training sessions required to achieve the criteria for completing PAL. The learning index (L) was estimated as follows: $L = (An - En)/(An + En)$, where En and An are the number of adjusted errors and attempts to the success, respectively, in the same session. Errors are made in PAL when the subject selects a box that does not contain the target stimulus. Important to consider that subjects failing at any stage of the test have had less opportunity to make errors than subjects who complete the test. Adjusted errors measure attempts to compensate for this. Adjusted errors for 1 shape measure the total number of errors made at the two 1-pattern stages (when there is a stimulus in one of the 6 boxes), with an adjustment added for those who have not completed the first stage. Subjects not reaching the second one-pattern stage are allocated the score 18 (one for each error made and an adjustment of 8). The maximum value for this measure (if the subject makes all possible responses incorrectly) is 19. The number of attempts to success is estimated by calculating the total number of trials required (maximum score = 10 trials per stage) to locate all the patterns correctly in all stages attempted, and dividing the result by the number of successfully completed stages. For detailed information and definitions, see http://www.cambridgecognition.com/tests/paired-associates-learning-pal.

Subjects had to achieve $L \geq 0.5$ in three consecutive sessions to complete the PAL task. Because L is expected to increase as a function of the number of training sessions, we weighted L by the number of sessions necessary to reach the criteria, which gave the ratio L/S, where L is the learning index and S is the number of sessions. The L/S ratio was used to investigate potential correlations between PAL performance and microglial features.

Microglial morphometry

We first investigated the presence of morphological features shared by the microglia found in each area and layer of interest in our sample. Because medial and lateral perforant pathways transmit spatial and non-spatial information to the dentate gyrus, (Witter et al., 1989; Witter and Amaral, 1991) and the entorhinal cortex projects to the CA1-LMol layer too (Witter and Amaral, 1991; Dolorfo and Amaral, 1998), we selected our microglial sample for 3D reconstructions from those layers. We submitted all morphometric quantitative variables to an initial cluster analysis (tree clustering method, Euclidean distances, and complete linkage), which included all subjects. Cluster analysis or clustering is the task of grouping a set of objects of interest in such a way that objects in the same group (called a cluster) are more similar to each other than to those in other groups (clusters). Cluster analysis encompasses a number of different classification algorithms applied to a wide variety of research problems (Steele and Weller, 1995; Schweitzer and Renehan, 1997; Gomes-Leal et al., 2002; Rocha et al., 2007); they are mostly used when one does not have an a priori hypothesis about which objects belong to a specific cluster group. We applied this multivariate statistical procedure to our sample of microglia to search for potential microglial classes. The microglial classes suggested by cluster analysis were further assessed with a forward stepwise discriminant function analysis, performed with Statistica 7.0 (Statsoft, Tulsa, OK). Discriminant function analysis is used to determine which variables discriminate between two or more naturally occurring groups. The idea underlying this procedure is to determine whether groups differ with regard to the mean of a variable, and then to use that

variable to predict group membership. In the present study, we used this software to perform comparisons between a matrix of total variances and covariances. These matrices were compared via multivariate *F* tests to determine whether there were any significant differences (with regard to all variables) between groups. In the step-forward discriminant function analysis, the program builds a model of discrimination step-by-step. In this model, at each step, all variables are reviewed and evaluated to determine which variable contributes most to the discrimination between groups. We applied this procedure to determine morphometric variables that provided the best separation between the microglial classes suggested by the cluster analysis. In addition, the arithmetic mean and standard deviation were calculated for the variables chosen as the best predictors for the microglia groups. Parametric statistical analyses with *t*-tests were applied to compare microglial groups between individuals; one-way ANOVAs were used to compare the average of each morphometric feature between animals.

Results

Fig. 1 illustrates the learning rates for each subject in the first stage of the PAL task. Note the significant differences in learning rates between subjects. *M* and *S* completed the task at the 3rd and 5th training sessions, respectively, and *J* and *F* performed best at the 14th and 19th training sessions, respectively. There were significant individual differences in the capacity for sustained acquisition of the recognition of spatial location of objects over three consecutive sessions. Nevertheless, all subjects showed the ability to learn within each trial, and their performances improved with repeated stimulus location presentations (not illustrated). In this within-trial learning, all subjects achieved stage 2 of the PAL test, where they were required to recognize the spatial locations of two distinct objects.

After testing, the monkeys were sacrificed, and brains were sectioned for morphological analyses of the hippocampus. A series of rostral to caudal sections from the hippocampus and dentate gyrus regions is illustrated in Fig. 2A. Fig. 2B is a low power photomicrography from a rostral section to illustrate areas and layers of interest.

To select microglia from the target areas for 3-D reconstructions, we referred to a previous architectonical study of the hippocampus and dentate gyrus of *Cebus apella* (Guerreiro-Diniz et al., 2010). Microglia from *Cebus apella* were selected from the external and middle DG-Mol and from the lacunosum molecular layer of CA1 (CA1-LMol). In the selected sections, the margins of the DG-Mol and of the CA1-LMol could be clearly distinguished under Nissl counterstaining. A total of 266 microglial cells were digitally reconstructed in three dimensions from dentate gyrus sections of *Cebus apella*. We selected microglia from external and middle thirds of the DG-Mol and from the CA1-LMol (Fig. 2B).

We analyzed 268 microglia from the dentate gyrus of all subjects (*F*, $n = 72$; *M*, $n = 73$; *S*, $n = 58$; and *J*, $n = 65$). Microglia were reconstructed from both rostral (172) and caudal (96) regions

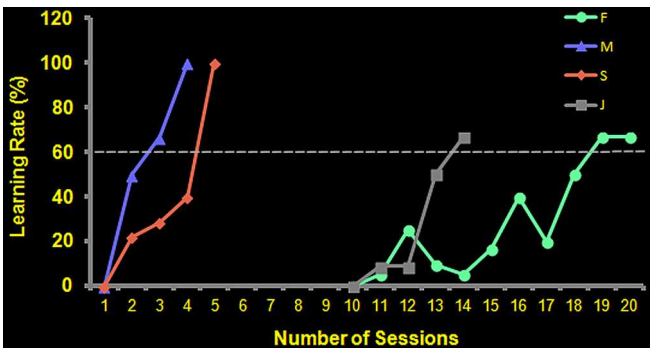

Fig. 1. Learning rates for each subject in the first stage of the PAL task. A normalized scale expresses the learning rate in percentage values as a function of the number of sessions. An arbitrary value of 60% was set as the minimum learning rate value to be achieved by each subject, before the behavioral assessment ended. Individual monkeys are designated *F*, *J*, *M*, and *S*.

of the DG-Mol. We performed a cluster analysis (tree clustering method) based on measurements of 22 morphometric features. The results suggested that our sample comprised two main classes of microglia, designated types I and II (Fig. 3). On average, compared to type II, type I microglia showed, shorter, thinner branches, smaller surface areas, smaller planar angles, less tortuosity, a higher density of branches, and less complexity (lower k-dim; Fig. 3). To determine which variables best discriminated between types I and II microglia, we performed a forward stepwise discriminant analysis. The discriminant model included the following parameters: tolerance (0.01); *F* to enter (1.00); *F* to remove (0.00); number of steps (22) at each step. After 12 steps, the classification algorithm retained the following variables: number of segments/mm ($p < 10^{-6}$), length of segments ($p = 0.00001$), fractal dimension ($p = 0.000173$), base diameter of the primary branches ($p = 0.000588$), planar angle ($p = 0.002532$), surface area ($p = 0.012866$), and branch volume ($p = 0.032625$), as the best predictors of class membership.

Similar cluster and discriminant analyses were applied to compare microglial morphology from the rostral and caudal regions of the dentate gyrus. In both cases, the results showed that the sampled microglia from those regions also comprised two main classes of microglia. To determine which variables best discriminated between microglia types I and II in the rostral and caudal regions, we performed another forward stepwise discriminant analysis. For the rostral region, after 14 steps, the classification algorithm retained the following variables: number of segments/mm ($p < 10^{-6}$), length of segments ($p = 0.000769$), fractal dimension ($p = 0.000029$), base diameter of the primary branches ($p = 0.000004$), planar angle ($p = 0.025154$), branch volume ($p = 0.050539$), tortuosity ($p = 0.003223$), and solidity ($p = 0.045904$) as the best predictors of class membership. For the caudal region, after 7 steps, the classification algorithm retained the following variables: number of segments/mm ($p = 0.000001$), length of segments ($p = 0.000019$), fractal dimension ($p = 0.008549$), base diameter of the primary branches ($p = 0.000098$), varicosities ($p = 0.024209$), and solidity ($p = 0.032092$). Although these two regions shared five predictive morphological variables (segments/mm, base diameter of primary branch, branch length, fractal dimension, and solidity), we found that significant linear correlations between PAL performance and microglial morphology were mainly limited to the rostral region. Indeed, the rostral region showed six distinct morphological correlations with PAL performance, one morphological feature from the branches (base diameter of the primary branches), and five from the cell soma (soma perimeter, soma area, aspect ratio, and the minimum and maximum Feret diameters) whereas the caudal region showed only one soma feature (Feret min); see Table 2 for details.

In the rostral region of the dentate gyrus, we found that, compared to type II microglia, type I microglia were, on average, significantly smaller, with thinner branches, less tortuosity, more ramified, and less complex (lower k-dim). When the average DG-Mol microglia of each monkey were compared with Types I and II, we found that F and J monkeys showed more similarity to type II microglia, and *M* and *S* monkeys showed more similarity with type I microglia. Furthermore, *F* samples were dominated by features of type II, and *J* microglial samples did not show any morphological predominance (Tables 3 and 4). On average, the *M* and *S* microglial samples displayed 17 and 14 morphological similarities, respectively, with type I microglia (Table 3); and *F* and *J* showed 18 and 11 morphological similarities, respectively, with type II (Table 4).

The rostral samples were also subjected to a separate cluster analysis. This analysis showed that, among the samples from *M* and *S* monkeys, 80.5% (33 in 41) and 92.7% (38 in 41), respectively, of the reconstructed microglia were classified as type I; in microglial

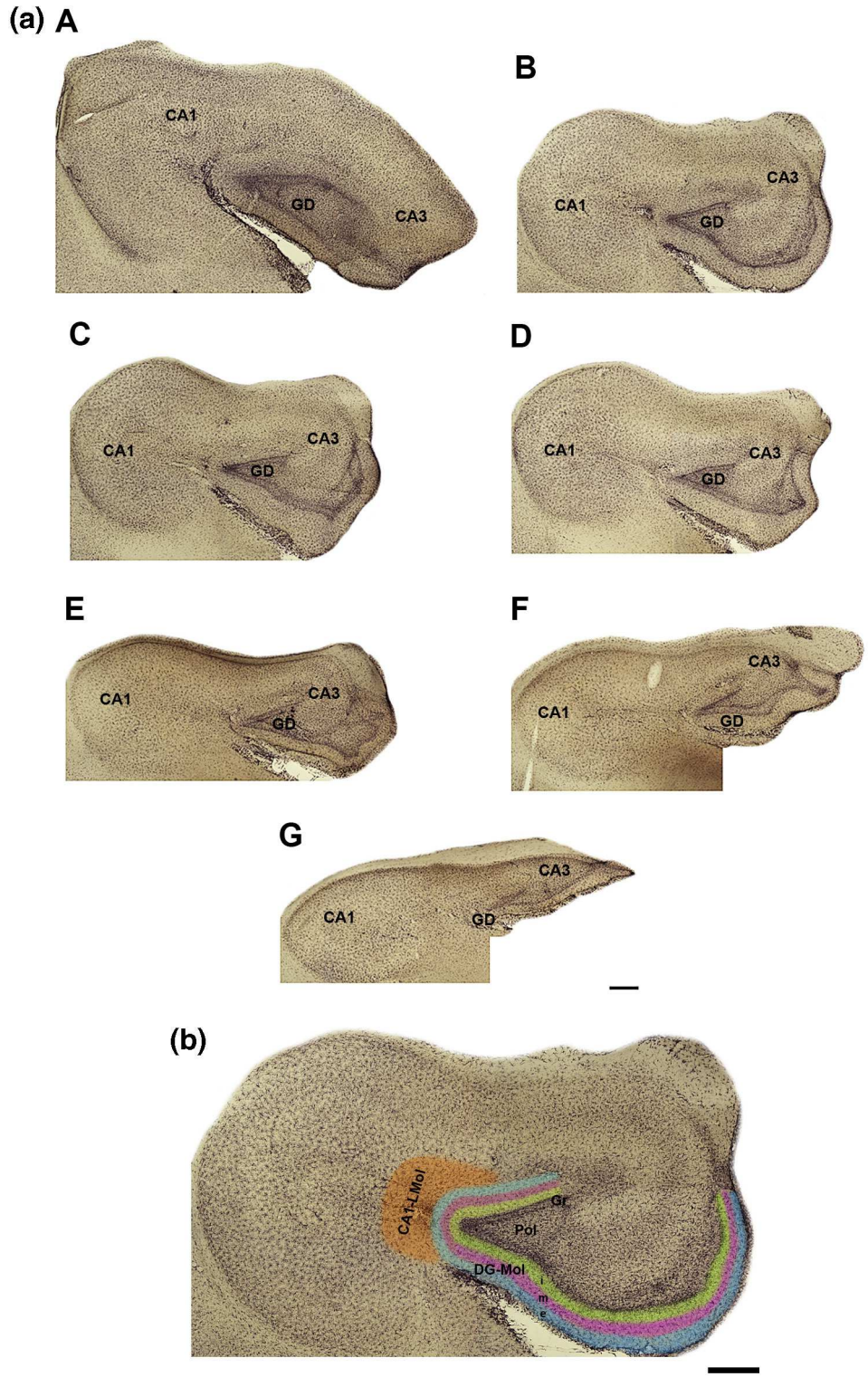

Fig. 2. (A). Low-power pictures of a series of IBA1-immunolabeled, rostro-caudal coronal sections from the hippocampus and dentate gyrus of *Cebus apella*. (A) Lowpower images (A)–(F) show serial sections that progress from the rostral (top) to the caudal (bottom) regions of the hippocampus, at 1.0 mm intervals. GD indicates the dentate gyrus. (B) Medium power pictures of areas and layers of interest in one of the serial sections used for selecting microglia for three-dimensional reconstructions. CA1-LMol = lacunosum molecular layer of CA1; Gr = dentate gyrus granular layer; Pol = polymorphic layer of dentate gyrus; DG-Mol = molecular layer of dentate gyrus; i, m, e = internal, middle, and external thirds of DG-Mol. Scale bars for both low and medium power images: 500 μm.

samples from *F* and *J*, the numbers of type I microglia corresponded to 31.4% (16 in 51) and 66.7% (26 in 39), respectively.

Next, we performed a discriminant analysis of the variables that significantly contributed to cluster formation in the caudal (Fig. 4A), rostral (Fig. 4B), and global (Fig. 4C) regions of the DG. Among the caudal and global microglial samples, the subjects that performed better (*S* and *M*) on the PAL-test were not well distinguished from those that performed worse (*F* and *J*). In contrast, in the rostral sample (4B), the subjects with best performance were mostly grouped to the left and those with worst performance were grouped to the right of the ordinate axis.

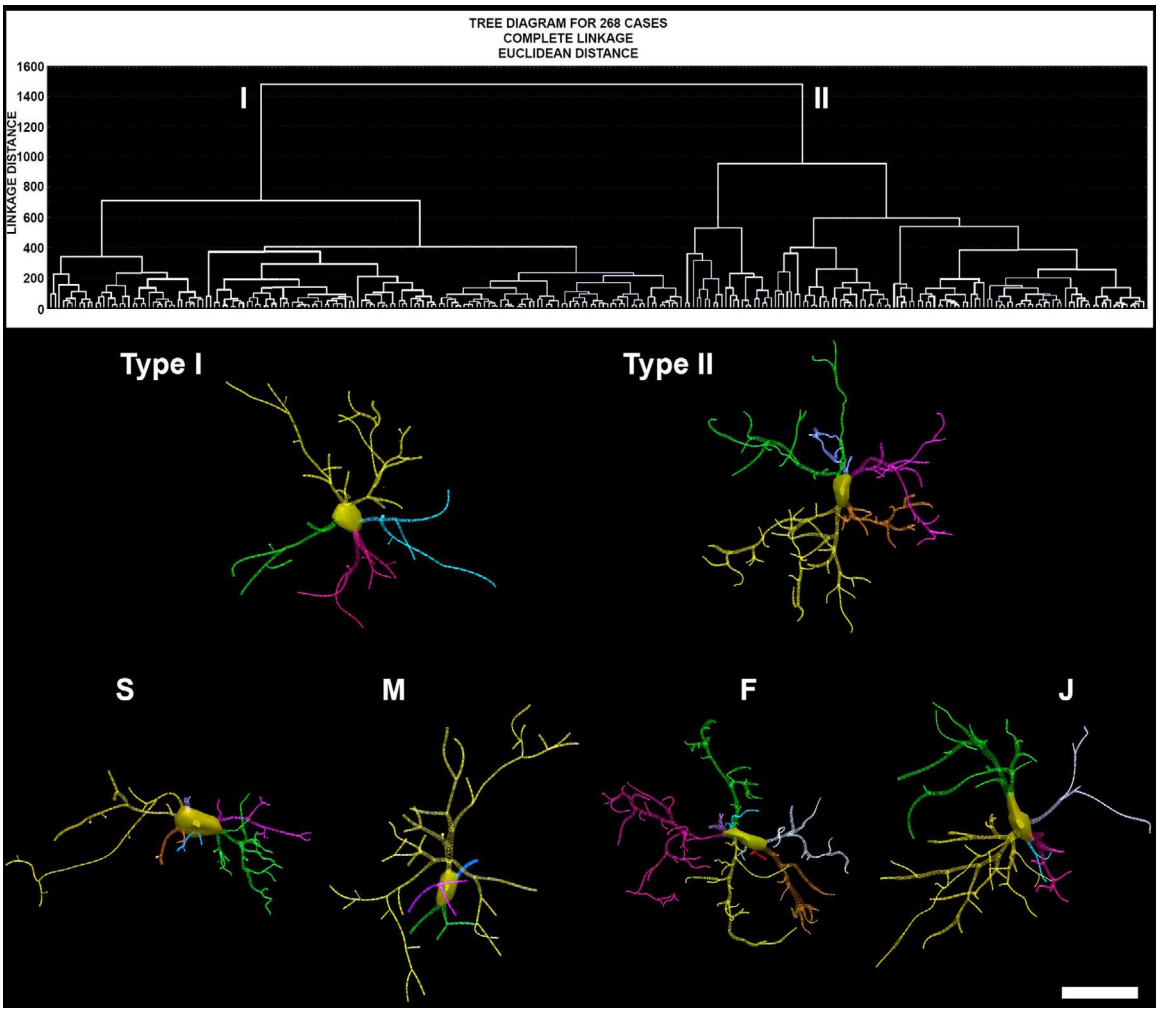

Fig. 3. Dendrogram of cluster analysis results (tree clustering method) and corresponding representative three-dimensional reconstructions. (*Top*) dendrogram groupings of 268 dentate gyrus microglia from all four subjects indicated 2 main microglial types (I and II). Microglia were reconstructed from both rostral (172) and caudal (96) regions of dentate gyrus, and cluster analysis was based on 22 microglia morphometric features. (*Middle*) microglial reconstructions represent the average values of morphologic features for types I and II microglia. (*Bottom*) microglial reconstructions represent the average values of morphologic features for *S*, *M*, *F* and *J* monkeys. Note close similarity between *S* and *M* average microglia with type I and between *F* average microglia with type II. *J* average microglia seems to be in an intermediate position.

In the lacunosum molecular of CA1 we analyzed 189 microglia (*F*, $n = 51$; *M*, $n = 50$; *S*, $n = 38$; and *J*, $n = 50$) and no simple correlations were found between PAL performance and the microglial morphological features in the CA1-LMol. Many morphological features of microglia from the rostral regions of the CA1- LMol and DG-Mol were remarkably similar in *F* and *J* subjects. Indeed, 20 of 21 morphological features were similar between the CA1-LMol and DG-Mol in the *F* monkey, and 16 of 21 were similar between regions in the *J* monkey (two-tail *t*-test $p \geq 0.05$). In contrast, microglia from these regions were quite different in *M* and *S* monkeys. Indeed, 15 and 12 of the total 21 morphological features were significantly different between the rostral CA1-LMol and DG-Mol regions in *M* and *S* subjects, respectively (two-tail *t*-test $p < 0.05$).

Fig. 5 illustrates serial microglial photomicrographs in different focus planes placed at 2 μm intervals and their correspondent

Table 2
Linear correlations between performances on paired associates learning task and microglial morphological features from rostral and caudal regions of dentate gyrus. The best performance (*M*) was considered 100%, and the others (*S*, *F* and *J*) were proportionally estimated as a function of the learning rate of each one. R^2 and *p* values correspond to the coefficient of determination and the level of statistical significance of the correlation analysis. No correlations were found between type II microglia and PAL performances.

			Rostral type I			
	M	*S*	*F*	*J*	R^2	*p*
Learnig rate	100%	80%	14%	16%		
Base diameter media (μm)	0.737	0.727	1.048	0.968	93.09%	0.035
Soma perimeter (μm)	26.49	27.267	30.775	32.137	93.24%	0.034
Soma area (μm^2)	41.56	41.57	50.361	48.657	95.46%	0.023
Feret max (μm)	9.272	9.861	11.285	11.47	98.50%	0.007
Feret min (μm)	6.076	6.064	6.42	6.5	92.00%	0.04
Aspect ratio	1.544	1.665	1.771	1.794	92.02%	0.04
			Caudal type I			
Feret min (μm)	6.073	5.987	6.791	6.725	92.71%	0.037

Table 3
Similarities and differences of microglial morphology from *M* and *S* monkeys with type I and type II microglia morphological features of the global sample. Numbers indicate mean ± standard errors of each parameter and *p* values the level of significance of each comparison. The first two rows exhibit mean values for types I and II morphometric features from the global microglial sample ($n = 268$) and the subsequent four rows exhibit the comparisons between *M* and *S* monkeys (*M*, $n = 73$; *S*, $n = 58$) with the global sample. Non-significant (ns) differences for each comparison highlight similarities between each morphometrical feature of the mean microglia of each monkey and types I and II microglia from the global sample.

	Branch length media (μm)	Branch length total (μm)	Tortuosity	Surface area (μm²)	Branch volume (μm³)	Primary base diameter (μm)	Number of Varicosities	Number of segments	Number of trees	Segments/ mm	Fractal dimension	Planar angle
Type I mean s.e.m.	6.294 ± 0.114	380.860 ± 7.624	1.126 ± 0.0039	613.261 ± 10.805	99.767 ± 2.670	0.800 ± 0.017	4.956 ± 0.249	63.075 ± 1.688	5.208 ± 0.154	166.655 ± 2.869	1.054 ± 0.002	46.531 ± 0.417
Type II mean s.e.m.	7.073 ± 0.112	555.967 ± 13.199	1.161 ± 0.005	1072.155 ± 19.467	217.919 ± 5.818	1.033 ± 0.020	9.330 ± 0.571	80.706 ± 2.346	6.138 ± 0.206	145.176 ± 2.281	1.079 ± 0.003	47.926 ± 0.419
M × type I	ns	433.392 ± 14.305 $p = 0.0015$	ns	702.638 ± 26.418 $p = 0.0023$	ns	ns	ns	ns	ns	ns	1.068 ± 0.003 $p < 0.0001$	ns
M × type II	6.423 ± 0.093 $p < 0.0001$	433.392 ± 14.305 $p < 0.0001$	1.127 ± 0.006 $p < 0.0001$	702.638 ± 26.418 $p < 0.0001$	115.947 ± 8.297 $p < 0.0001$	0.789 ± 0.033 $p < 0.0001$	5.863 ± 0.448 $p < 0.0001$	67.877 ± 2.142 $p < 0.0001$	5.288 ± 0.252 $p = 0.01$	157.955 ± 2.223 $p = 0.0001$	1.068 ± 0.003 $p = 0.008$	45.757 ± 0.607 $p = 0.0029$
S × type I	5.100 ± 0.104 $p < 0.0001$	417.921 ± 14.408 $p = 0.017$	1.097 ± 0.003 $p < 0.0001$	664.086 ± 21.439 $p = 0.0229$	ns	0.711 ± 0.013 $p < 0.0001$	ns	82.569 ± 2.843 $p < 0.0001$	ns	200.479 ± 3.933 $p < 0.0001$	1.062 ± 0.003 $p = 0.0303$	ns
S × type II	5.100 ± 0.104 $p < 0.0001$	417.921 ± 14.408 $p < 0.0001$	1.097 ± 0.003 $p < 0.0001$	664.086 ± 21.438 $p < 0.0001$	101.664 ± 4.088 $p < 0.0001$	0.711 ± 0.013 $p < 0.0001$	4.690 ± 0.489 $p < 0.0001$	ns	ns	200.479 ± 3.933 $p < 0.0001$	1.062 ± 0.003 $p < 0.0001$	45.591 ± 0.477 $p = 0.0007$

	Perimeter (μm)	Soma area (μm²)	Feret max (μm)	Feret min (μm)	Aspect ratio	Compactness	Convexity	Form factor	Roundness	Solidity
Type I	28.693 ± 0.453	43.628 ± 0.937	10.100 ± 0.171	6.176 ± 0.083	1.661 ± 0.030	0.746 ± 0.007	0.926 ± 0.004	0.677 ± 0.010	0.564 ± 0.010	0.930 ± 0.005
Type II	31.881 ± 0.810	51.366 ± 1.537	11.637 ± 0.343	6.550 ± 0.100	1.805 ± 0.055	0.713 ± 0.010	0.935 ± 0.004	0.661 ± 0.013	0.519 ± 0.014	0.912 ± 0.007
M × type I	ns	ns	ns	ns	ns	ns	ns	0.713 ± 0.011 $p = 0.0206$	ns	0.955 ± 0.005 $p = 0.0005$
M × type II	27.518 ± 0.546 $p < 0.0001$	42.891 ± 1.319 $p < 0.0001$	9.733v ± 0.230v$p < 0.0001$	6.075v ± 0.106v$p = 0.0019$	1.617 ± 0.037 $p = 0.0054$	0.764 ± 0.009 $p = 0.0002$	ns	0.713 ± 0.012 $p = 0.004$	0.590 ± 0.014 $p = 0.0006$	0.955 ± 0.005 $p < 0.0001$
S × type I	ns	ns	ns	ns	ns	ns	ns	ns	ns	ns
S × type II	27.741 ± 0.617 $p < 0.0001$	41.623 ± 1.362 $p < 0.0001$	9.835 ± 0.259 $p < 0.0001$	6.080 ± 0.146 $p = 0.0078$	ns	0.749 ± 0.013 $p = 0.0313$	ns	ns	0.571 ± 0.019 $p = 0.0266$	ns

Table 4
F and *J* microglial similarities and differences with type I and type II microglia from the dentate gyrus global sample of all monkeys. Numbers indicate mean ± standard errors and p values of each comparison. The first two rows exhibit mean values for types I and II morphometric features from global microglial sample ($n = 268$) and the subsequent 4 rows exhibit the mean, standard errors and p values to highlight significant differences between *F* and *J* monkeys microglial samples and global microglia. Non-significant differences (ns) highlight similarities between the mean values of each monkey and global sample and types I and II.

	Branch length media (μm)	Branch length total (μm)	Tortuosity	Surface area (μm^2)	Branch volume (μm^3)	Base diameter media (μm)	Number of varicosity	Number of segments	Number of	Segments/ mm	Fractal dimension	Planar angle
Type I mean s.e.m.	6.294 ± 0.114	380.860 ± 7.624	1.126 ± 0.0039	613.261 ± 10.805	99.767 ± 2.670	0.800 ± 0.017	4.956 ± 0.249	63.075 ± 1.688	5.208 ± 0.154	166.655 ± 2.869	1.054 ± 0.002	46.531 ± 0.417
Type II mean s.e.m.	7.073 ± 0.112	555.967 ± 13.199	1.161 ± 0.005	1072.155 ± 19.467	217.919 ± 5.818	1.033 ± 0.020	9.330 ± 0.571	80.706 ± 2.346	6.138 ± 0.206	145.176 ± 2.281	1.079 ± 0.003	47.926 ± 0.419
F × type I	7.014 ± 0.123 $p < 0.0001$	473.938 ± 15.497 $p < 0.0001$	1.161 ± 0.005 $p < 0.0001$	937.994 ± 33.161 $p < 0.0001$	199.702 ± 8.455 $p < 0.0001$	1.064 ± 0.0183 $p < 0.0001$	7.792 ± 0.548 $p < 0.0001$	ns ns ns	5.986 ± 0.257 $p = 0.0076$	145.451 ± 2.369 $p < 0.0001$	1.062 ± 0.003 $p = 0.0287$	ns
F × Type II	Ns	473.938 ± 15.496 $p = 0.0001$	ns	937.994 ± 33.161 $p = 0.0007$	ns	ns	7.792 ± 0.548 $p = 0.054$	67.833 ± 2.405 $p = 0.0003$	ns	ns	1.062 ± 0.003 $p < 0.0001$	ns
J × Type I	7.723 ± 0.176 $p < 0.0001$	479.332 ± 23.660 $p = 0.0002$	1.172 ± 0.007 $p < 0.0001$	877.359 ± 40.071 $p < 0.0001$	167.339 ± 8.226 $p < 0.0001$	0.990 ± 0.023 $p < 0.0001$	8.369 ± 0.8062 $p = 0.0001$	ns	ns	133.712 ± 3.011 $p < 0.0001$	1.065 ± 0.0055 $p = 0.0278$	49.450 ± 0.654 $p = 0.0003$
J × Type II	7.723 ± 0.176 $p = 0.0014$	479.332 ± 23.660 $p = 0.0056$	ns	877.359 ± 40.071 $p < 0.0001$	167.339 ± 8.226 $p < 0.0001$	ns	ns	64.585 ± 3.933 $p = 0.0006$	5.477 ± 0.247 $p = 0.0461$	133.712 ± 3.011 $p = 0.0028$	1.065 ± 0.005 $p = 0.0109$	49.450 ± 0.654 $p = 0.0419$
	Soma perimeter (μm)	Soma area (μm^2)	Feret max (μm)	Feret min (μm)	Aspect ratio	Compactness	Convexity	Form factor	Roundness	Solidity		
Type I	28.693 ± 0.453	43.628 ± 0.937	10.100 ± 0.171	6.176 ± 0.083	1.661 ± 0.030	0.746 ± 0.007	0.926 ± 0.004	0.677 ± 0.010	0.564 ± 0.010	0.930 ± 0.005		
Type II	31.881 ± 0.810	51.366 ± 1.537	11.637 ± 0.343	6.550 ± 0.100	1.805 ± 0.055	0.713 ± 0.010	0.935 ± 0.004	0.661 ± 0.013	0.519 ± 0.014	0.912 ± 0.007		
F × Type I	31.018 0.768 $p = 0.0071$	50.540 1.831 $p = 0.0011$	11.243 0.319 $p = 0.002$	6.543 0.124 $p = 0.0149$	ns	ns	ns	ns	ns	ns		
F × Type II	ns	ns	ns	ns	ns	ns	ns	ns	ns	ns		
J × Type I	33.632 ± 1.203 $p = 0.0002$	51.564 ± 1.9715 $p = 0.0004$	12.060 ± 0.491 $p = 0.0003$	6.597 ± 0.135 $p = 0.0078$	1.861 ± 0.079 $p = 0.0197$	0.691 ± 0.012 $p < 0.0001$	ns ns ns	0.604 ± 0.017 $p = 0.0001$	0.486 ± 0.015 $p < 0.0001$	0.891 ± 0.010 $p = 0.0007$		
J × Type II	ns	ns	ns	ns	ns	ns	0.915 ± 0.007 $p = 0.0169$	0.604 ± 0.017 $p = 0.0101$	ns	ns		

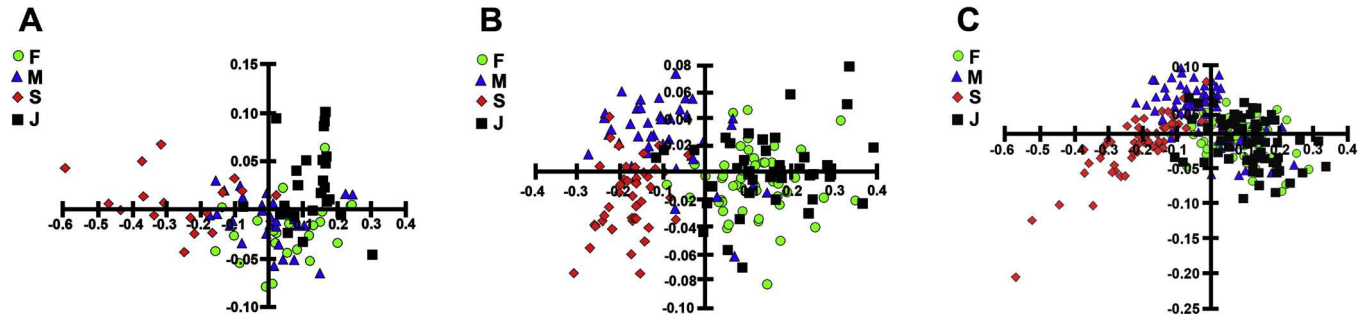

Fig. 4. Graphical representations of discriminant analysis, based on variables that significantly contributed to cluster formation. Average morphometric measures (*Y*-axis) and the correlated PAL performance (*X*-axis) are shown for microglia from the (A) caudal, (B) rostral, (C) and global regions of the dentate gyrus. Each symbol represents one microglial morphometric feature, and different colors and shapes indicate the different subjects.

three-dimensional reconstructions of a microglia with morphological features closer to the microglial mean values of each monkey. As compared to *F* and *J* (rows C and D), *S* and *M* microglia (rows A and B) show on average, more similarity with type I microglia.

Fig. 6 are graphic representations of mean values and correspondent standard errors of type I and type II microglial morphological features from rostral (A–F), caudal (G, H) or global sample (I–L). We selected morphometric features that exhibited linear and/or non-linear correlations with PAL performance. Note that as compared to caudal region the rostral region of DG-Mol showed the highest number of variables correlated with spatial learning. Indeed we found 6 morphometrical features correlated with PAL scores in the rostral region and only 2 in caudal. When correlation analysis is done with the global sample (rostral plus caudal) we found significant correlation with 4 parameters. Also, the morphological features of types I and II microglia showed similar values in different regions of interest. On average, compared to type II, type I microglia showed smaller primary branch diameters, smaller branch planar angles, lower complexity (smaller K-dim), smaller soma areas and perimeters, and smaller Feret maximum and minimum diameters.

Discussion

Four capuchin-monkeys (*Cebus apella*) were submitted to stage 1 of paired associates learning test of the CANTAB battery and an index of their performances on spatial learning and memory was estimated. Two subjects (*M* and *S*) complete the task after three and four training sessions and two others (*J* and *F*) only after 13 and 19 sessions respectively. After behavioral tests animals were euthanized and three-dimensional reconstructions of microglia from outer and middle thirds of the molecular layer of the dentate gyrus and from CA1 lacunosum molecular layer were performed. Using cluster and discriminant analysis on morphometric features we identified the occurrence of at least two large and distinct groups of microglial morphologies designated types I and II. In a search for possible correlations between PAL performances and morphological features of microglia we mainly found significant correlations with type I from DG-Mol rostral region, a few correlations with type II of caudal region and no correlations with CA1 microglial morphology. The results seem to be coherent with previous proposed regional specializations for rostral and caudal regions of monkey

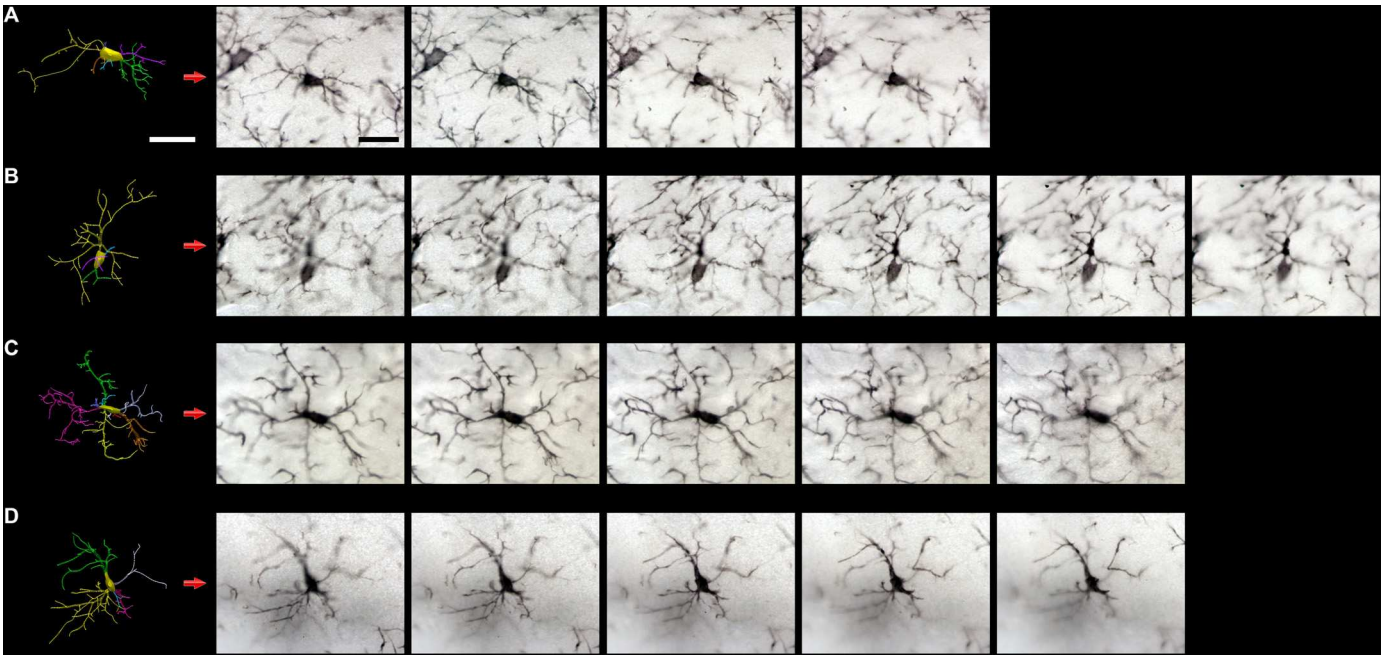

Fig. 5. Serial microglial photomicrographs in different focus planes placed at 2 μm intervals and correspondent three-dimensional reconstructions of microglia from rostral region of dentate gyrus of each subject. Microglia examples from *F*, *M*, *S* and *J* subjects are illustrated in (A), (B), (C) and (D) rows, respectively. Scale bar = 10 μm.

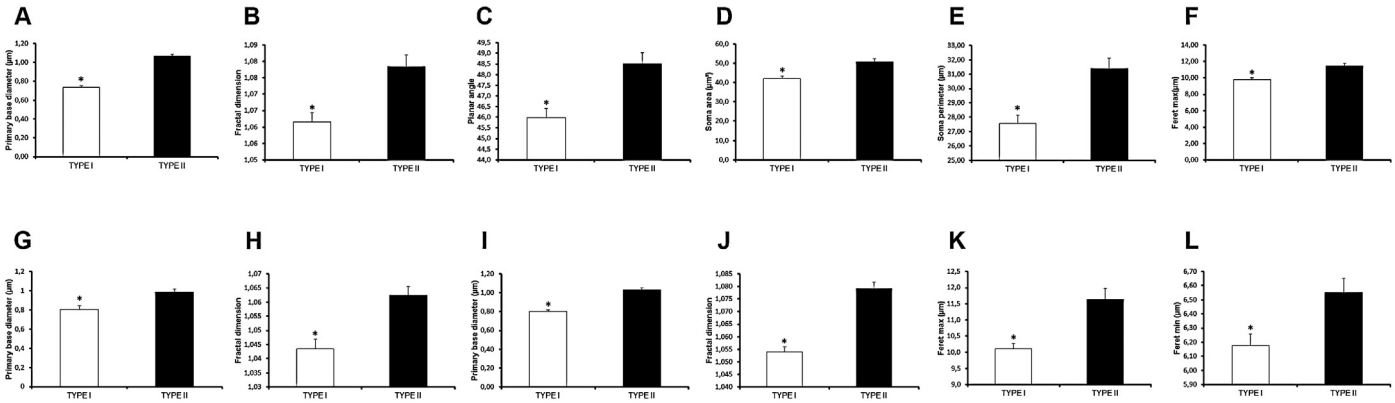

Fig. 6. Differences in morphological features between types I and II microglia. Morphological variables were selected from type I microglia that exhibited significant correlations with PAL performances. Types I and II microglia from two regions of the DG-Mol were compared for (A–(F) six rostral variables, (G), (H) two caudal variables, and (I)–(L) four global (rostral plus caudal) variables. * Indicates significant differences between types I and II microglia. Bars and whiskers represent the mean and standard error, respectively.

dentate gyrus and suggest that type I microglia from rostral region may be associated with spatial learning and memory consolidation in the *Cebus apella*.

Spatial learning and memory in Cebus apella

The present report using the paired associates learning task from CANTAB battery confirmed previous findings that the *Cebus apella* meets all the behavioral substrates required for the use of visuo-spatial memory to search for objects of interest (Garber and Paciulli, 1997; Janson, 1998; Potì et al., 2010; Pan et al., 2011), including the small scale, touch-sensitive computer screen. PAL tasks have been used to investigate the role of the hippocampus in incrementally encoding associations between different stimuli (Blackwell et al., 2004; Skolimowska et al., 2011; Junkkila et al., 2012; Sanchez-Ramos et al., 2012). Our findings provided a basis for new comparisons between New and Old World primates (Taffe et al., 2002; Spinelli et al., 2004) and with human performance (Nagahara et al., 2010). Despite significant individual differences in capability in the acquisition of the recognition memory aspects of the PAL task, all Cebus monkeys evidenced the ability to learn within trial, completing stages 1 to 3. However, as compared to *Macaca mulatta*, which completed stage 3 (three stimulus, three locations) in all sessions (Taffe et al., 2002; Von Huben et al., 2006), *Cebus apella* performances between sessions were sustained only for stage 1 (one stimulus, one location). Healthy humans typically complete all stages (1–6) of the PAL task (Robbins et al., 1994; Lee et al., 2013).

It is also important to discuss possible reasons to explain why are the performances of monkeys *M* and *S* so different from that of *F* and *J* in the PAL-task? In a previous report investigating spatial working memory in non-human primates, *Macaca fascicularis* adult females performed better than their adult male counterparts and cage-bred subjects performed better than island-bred (natural environment) individuals (Darusman et al., 2014). In the present report all subjects were maintained in captivity and females revealed better performances than males. Since females were 2 and males were 4 years old, and on average, Cebus monkeys reach sexual maturity at 5 years old, and live on average 40 years in captivity, both males and females used in the present study were sexually immature and infants (Wirz and Riviello, 2008). Thus, our sample and that of *Macaca fascicularis*, do not allow direct comparisons postponing possible generalizations about gender, species or age influences on spatial memory task performances in the *Cebus apella*.

Hippocampus, microglial cells and episodic-like memory

Episodic-like memory allows an unambiguous distinction between new and familiar objects; see (Eichenbaum et al., 2012) for recent review. To cope with these tasks the brain needs to accentuate the differences between the old and new experiences before coding occurs, so you can distinguish those (Schmidt et al., 2012). For that purpose, medial and lateral perforant pathways transmit to dentate gyrus, spatial and non-spatial information that would be necessary to recognize object placement (Where?), identity (What?) and timing (When?). Lateral portions of the entorhinal cortex project to caudal levels of the dentate gyrus and hippocampus, whereas medial portions of the entorhinal cortex project to rostral levels (Witter et al., 1989; Witter and Amaral, 1991). It has also been demonstrated that entorhinal cortex of Rhesus monkey and rat also projects to the lacunosum molecular layer of CA1 (Witter and Amaral, 1991; Dolorfo and Amaral, 1998) and those synapses, at least in rats, exhibit synaptic plasticity associated with allocentric spatial learning and memory (Remondes and Schuman, 2002; Remondes and Schuman, 2003; Remondes and Schuman, 2002, 2003 and 2004; Langston et al., 2010).

Although this study is explicitly correlational, it raises the opportunity to provide hypotheses about the relationships between microglial morphology and spatial learning. Is it possible that these findings can be attributed to individual differences in the subjects, i.e., the quick-learning monkeys already had Type I microglia and the slower monkeys already had Type II microglia, influencing their success? Because microglial Types I and II in the DG rostral samples were asymmetrically distributed with a higher proportion of Type I among the samples from *M* (80.5%) and *S* (92.7%) as compared with the samples from *F* (31.4%) and *J* (66.7%) monkeys and *M* and *S* show the best performances it would be possible that learning-dependent synapse formation may be enhanced by type I microglia. One possibility to test this hypothesis would be to investigate learning-dependent synaptic formation combining electronic microscopy and stereological analysis in quick and slow-learning monkeys.

Another possibility would be that the degree of neuronal signaling during learning and memory consolidation could be one of the reasons to explain microglial morphology so distinct in monkeys that learned quickly. In line with this possibility recent findings revealed that microglia is associated with important physiological functions in learning and memory by promoting learning-related synapse formation through BDNF signaling

(Parkhurst et al., 2013). Indeed, after training to learn and remember the spatial location of an object, synapse remodeling in the dorsal DG is already evident 6 h later in DG-Mol layer and that remodeling is microglia-dependent (Scully et al., 2012). In addition it has been described that the functional microglial status is associated with a combination of extracellular changes in neuronal activity (Tremblay et al., 2010, 2011; Wake et al., 2011, 2013), chemokine signaling (Liang et al., 2009) and purinergic signaling (Davalos et al., 2005; Dibaj et al., 2010; Fontainhas et al., 2011; Ohsawa and Kohsaka, 2011). Among these influences neuronal activity would be a good candidate to regulate of microglial physiology as among microglial functions are the maintenance of synapses and release of trophic factors (Wong et al., 2011). Synchronized with the levels of neural activity which increases glutamatergic ionotropic neurotransmission, distinct microglial morphological changes could be associated with distinct GABA activity through the release of extracellular ATP (Fontainhas et al., 2011; Wong et al., 2011). This control of microglial morphology by different forms of neurotransmission occurs within minutes and seem to depend on mutual communication between neurons and microglia. In line with these observations it has been demonstrated that interleukin1β, a pro-inflammatory cytokine produced by microglia during learning and memory tasks, seem to be necessary at physiological levels for hippocampus-dependent tasks, whereas concentrations that are either too low or too high impair memory (Schneider et al., 1998; Ross et al., 2003; Goshen et al., 2007).

Thus, it may be possible that type I microglia may be more sensitive to neuronal signaling and start synapse remodeling earlier than type II microglia and in doing so, quick-learning individuals with a higher proportion of type I microglia starts learning and memory consolidation before slow-learning monkeys.

PAL tests have been used as an episodic memory test in humans (Robbins et al., 1994; de Jager et al., 2002; Juncos-Rabadán et al., 2014) and episodic-like memory test in non-human primates (Spinelli et al., 2004, 2006; Nagahara et al., 2010; Rodriguez et al., 2011).

In the present report M and S monkeys were able to learn and remember objects spatial location and completed PAL task in three and five training sessions respectively, whereas *F* and *J* subjects were able to do so only after 15 and 19 sessions. Because PAL performances of these monkeys were correlated with type I microglia from rostral DG-Mol but not with type II we suggest that type I microglia in the molecular layer of dentate gyrus may be important for spatial learning and memory consolidation. Since microglial type I morphological features from rostral and caudal DG-Mol but not from CA1-LMol were correlated with PAL performances we speculate that in both rostral (higher proportion) and caudal (lower proportion) regions of DG-Mol in *Cebus apella* may be occurring microglia-dependent synapse remodeling and that this event could be associated with spatial learning and memory (Scully et al., 2012).

In the present study, we found marked differences in the morphology of microglia in both the hippocampus and dentate gyrus finding a strong linear correlation between PAL performances and morphometric parameters of microglia from the molecular layer of the dentate gyrus of *Cebus apella*. In particular, some morphological features of type I microglia from rostral region of dentate gyrus exhibited coefficient of determinations (R^2 values) above 90% and significant *p* values ($p < 0.05$) for soma (area, perimeter, form factor and Feret max) and branches (base diameter of primary branch, fractal dimension, and planar angle) morphological parameters (Table 5). These findings seem consistent with evidence that the morphology of microglia can be used to characterize changes in their functional status (Karperien et al., 2013).

Another relevant point to be considered is that the outer and middle thirds of the molecular layer of the rostral and caudal dentate gyrus receive their inputs from the medial and lateral perforant pathways. Those axon terminals converge on the dendrites of the granule cells where their synapses seem to compete and cooperate as a function of the different distances that separate those from the soma of granular neurons (Hayashi and Nonaka, 2011). In the present report we described significant correlations between *Cebus apella* performances in PAL task and the morphology of microglia from the molecular layer of the dentate gyrus where presumably the activity of the perforant pathway would be more intense during visuospatial learning training sessions. We speculate that increased neurotransmission in those layers may contribute to change microglial morphology and that those microglial morphological changes may be necessary to the spatial learning and memory associated synaptic physiology. Coherently with this view the animals that showed better performance in PAL test showed on average, microglial morphological features quite distinct from those with lower performances. Although these findings constitute an indirect evidence they are consistent with the regional specialization of the hippocampal formation of *Cebus apella* (Guerreiro-Diniz et al., 2010) in all very much similar to that of Old World monkeys (Amaral and Lavenex, 2007) and humans (Clark and Squire, 2013).

Technical limitations

In the present report multivariate statistical analysis using morphometric parameters of microglia revealed at least two

Table 5
Linear correlations between performances on paired associates learning task and type I microglial morphological features from rostral and caudal regions of dentate gyrus. The best performance (*M*) was considered 100% e the others (*S*, *F* and *J*) were proportionally estimated as a function of the learning rate of each one. R^2 and *p* values correspond to the coefficient of determination and statistical significance of the correlation analysis.

	Rostral type I					
	M	*S*	*F*	*J*	R^2 (%)	*p*
Learnig rate100%	80%	14%	16%			
Base diameter media (μm)	0.64	0.72	0.87	0.90	97.20	0.0141
Fractal dimension	1.07	1.06	1.04	1.03	92.22	0.0397
Planar angle	45.44	45.47	47.61	47.77	95.86	0.0209
Soma perimeter (μm)	26.04	27.28	31.44	29.87	95.30	0.0238
Soma area (μm^2)	40.03	41.53	46.70	45.69	99.34	0.0036
Form factor	0.73	0.70	0.62	0.64	98.65	0.0068
Feret max (μm)	9.07	9.86	11.10	10.49	90.33	0.0495
	Caudal type I					
Fractal dimension	1.05	1.04	1.03	1.03	93.20%	0.0346
Compactness	0.74	0.74	0.71	0.70	94.00%	0.0304

morphologically distinct groups of microglia in the molecular layer of the dentate gyrus and in the lacunosum molecular of CA1 in all animals and type I but not type II revealed significant correlations with Cebus monkey performances in PAL test. Although the evidence in the present report is indirect we suggest that the functional contribution of each of these morphological groups of microglia might be different.

Microscopic, 3D reconstructions may be affected by mechanical factors associated with the vibratome sectioning and the dehydration procedure, which can induce non-uniform shrinkage in the *z*-axis of the sections (Hosseini-Sharifabad and Nyengaard, 2007). Thus, estimates of modifications in the x/y dimensions during tissue processing cannot be linearly extrapolated to the *z* dimension. These methodological constraints imposed limitations that must be taken into consideration when interpreting the results of the present study. However it must be emphasized that a reliable indication of severe shrinkage in *z* axis is the curling of branches, signifying that individual processes did not shrink at the same rate as the slice in which they are located. These effects tend to be of higher amplitude at the surface, decreasing in depth in the *z*-axis. This pattern, however, was not observed in microglia elected to be reconstructed in this study and our sample was taken from the middle region of the *z*-axis, where the impact of these changes are minor. More recently it has been demonstrated that in the *z*-axis (perpendicular to the cutting surface) sections shrink to approximately 25% of the cut thickness after dehydration and clearing (Carlo and Stevens, 2011). Based on those findings all microglial reconstructions of the present report were corrected for *z*-axis shrinkage in 75%. No corrections were applied to *X*/*Y* axes that did not change after histological dehydration and clearing.

Another limitation is related to the fact that no stereological procedures were performed to estimate the total number of each type of microglia in the target areas. However because the criteria to select microglia for three-dimensional reconstructions were systematically blind and random in all subjects, and the number of elements selected for reconstruction was rather wide (453 in total, 188 in the lacunosum molecular of CA1 and 268 in the outer and middle thirds of the molecular layer of the dentate gyrus) it is reasonable to suppose that no a priori sample bias was induced by the choice of objects of interest among subjects.

Regarding the correlations between behavior and morphometric variables of microglia found in this study it is important to keep in mind that although the coefficient of determination (R^2) or the coefficient of Pearson between behavioral tests and many of the morphometric variables were highly significant it only refers to a numerical relationship between the tested variables, not necessarily implying a cause-effect relationship. In the case of non-linear correlations the results of R^2 should be taken with caution because of the difficulty in complying with certain underlying assumptions to that coefficient (Ma et al., 2011).

Ethical statement

All procedures were carried out under the approval of the Institutional Ethics Committee for Animal Experimentation of the Federal University of Para, in accordance with NIH and Brazilian regulations for scientific procedures on animals. All efforts were made to minimize the number and suffering of the animals.

Acknowledgments

Supporting funds from Fundação de Amparo a Pesquisa do Pará—FADE$P; Pró-Reitoria de Pesquisa e Pós-Graduação da Universidade Federal do Pará EDITAL 02/2014–PIAPA Brazilian Research Council—CNPq grant number: 307749/2004-5 and 471077/2007-0 for CWPD and FINEP, Instituto Brasileiro de Neurociências—IBNnet

References

Amaral, D.G., Lavenex, P., 2007. Hippocampal neuroanatomy. In: Andersen, P., Morris, R.G., Amaral, D.G., Bliss, T., O'Keefe, J. (Eds.), The Hippocampus Book. Oxford University Press, New York, NY, pp. 37–114.

Benarroch, E.E., 2013. Microglia: Multiple roles in surveillance, circuit shaping, and response to injury. Neurology 81, 1079–1088.

Blackwell, A.D., Sahakian, B.J., Vesey, R., Semple, J.M., Robbins, T.W., Hodges, J.R., 2004. Detecting dementia: novel neuropsychological markers of preclinical Alzheimer's disease. Dement. Geriatr. Cogn. Disord. 17, 42–48.

Carlo, C.N., Stevens, C.F., 2011. Analysis of differential shrinkage in frozen brain sections and its implications for the use of guard zones in stereology. J. Comp. Neurol. 519, 2803–2810.

Clark, R.E., Squire, L.R., 2013. Similarity in form and function of the hippocampus in rodents, monkeys, and humans. Proc. Natl. Acad. Sci. U.S.A. 110 (Suppl. 2) 10365–10370.

Darusman, H.S., Kalliokoski, O., Sajuthi, D., Schapiro, S.J., Gjedde, A., Hau, J., 2014. The success rate in a complicated spatial memory test is determined by age, sex, life history and search strategies in cynomolgus monkeys. In Vivo 28, 741–750.

Davalos, D., Grutzendler, J., Yang, G., Kim, J.V., Zuo, Y., Jung, S., Littman, D.R., Dustin, M.L., Gan, W.B., 2005. ATP mediates rapid microglial response to local brain injury in vivo. Nat. Neurosci. 8, 752–758.

de Jager, C.A., Milwain, E., Budge, M., 2002. Early detection of isolated memory deficits in the elderly: the need for more sensitive neuropsychological tests. Psychol. Med. 32, 483–491.

Dibaj, P., Nadrigny, F., Steffens, H., Scheller, A., Hirrlinger, J., Schomburg, E.D., Neusch, C., Kirchhoff, F., 2010. NO mediates microglial response to acute spinal cord injury under ATP control in vivo. Glia 58, 1133–1144.

Dolorfo, C.L., Amaral, D.G., 1998. Entorhinal cortex of the rat: topographic organization of the cells of origin of the perforant path projection to the dentate gyrus. J. Comp. Neurol. 398, 25–48.

Dufour, V., Pascalis, O., Petit, O., 2006. Face processing limitation to own species in primates: a comparative study in brown capuchins, Tonkean macaques and humans. Behav. Processes 73, 107–113.

Eichenbaum, H., Sauvage, M., Fortin, N., Komorowski, R., Lipton, P., 2012. Towards a functional organization of episodic memory in the medial temporal lobe. Neurosci. Biobehav. Rev. 36, 1597–1608.

Facal, D., Rodríguez, N., Juncos-Rabadán, O., Manuel Caamaño, J., Sueiro, J., 2009. [Use of the Cambridge Neuropsychological Test Automated Battery for the diagnosis of mild cognitive impairment. A pilot study in a Spanish sample] Rev. Esp. Geriatr. Gerontol. 44, 79–84.

Fontainhas, A.M., Wang, M., Liang, K.J., Chen, S., Mettu, P., Damani, M., Fariss, R.N., Li, W., Wong, W.T., 2011. Microglial morphology and dynamic behavior is regulated by ionotropic glutamatergic and GABAergic neurotransmission. PLoS One 6, e15973.

Garber, P.A., Paciulli, L.M., 1997. Experimental field study of spatial memory and learning in wild capuchin monkeys (Cebus capucinus). Folia. Primatol. (Basel) 68, 236–253.

Gomes-Leal, W., Silva, G.J., Oliveira, R.B., Picanco-Diniz, C.W., 2002. Computer-assisted morphometric analysis of intrinsic axon terminals in the supragranular layers of cat striate cortex. Anat. Embryol. (Berl) 205, 291–300.

Gomez-Nicola, D., Perry, V.H., 2014. Microglial Dynamics and Role in the Healthy and Diseased Brain: A Paradigm of Functional Plasticity. Neuroscientist.

Goshen, I., Kreisel, T., Ounallah-Saad, H., Renbaum, P., Zalzstein, Y., Ben-Hur, T., Levy-Lahad, E., Yirmiya, R., 2007. A dual role for interleukin-1 in hippocampal-dependent memory processes. Psychoneuroendocrinology 32, 1106–1115.

Guerreiro-Diniz, C., de Melo Paz, R.B., Hamad, M.H., Filho, C.S., Martins, A.A., Neves, H.B., de Souza Cunha, E.D., Alves, G.C., de Sousa, L.A., Dias, I.A., Trévia, N., de Sousa, A.A., Passos, A., Lins, N., Torres Neto, J.B., da Costa Vasconcelos, P.F., Picanço-Diniz, C.W., 2010. Hippocampus and dentate gyrus of the Cebus monkey: architectonic and stereological study. J. Chem. Neuroanat. 40, 148–159.

Hanisch, U.K., Kettenmann, H., 2007. Microglia: active sensor and versatile effector cells in the normal and pathologic brain. Nat. Neurosci. 10, 1387–1394.

Hayashi, H., Nonaka, Y., 2011. Cooperation and competition between lateral and medial perforant path synapses in the dentate gyrus. Neural Netw. 24, 233–246.

Hosseini-Sharifabad, M., Nyengaard, J.R., 2007. Design-based estimation of neuronal number and individual neuronal volume in the rat hippocampus. J. Neurosci. Methods 162, 206–214.

Janson, C.H., 1998. Experimental evidence for spatial memory in foraging wild capuchin monkeys, Cebus apella. Anim. Behav. 55, 1229–1243.

Juncos-Rabadán, O., Pereiro, A.X., Facal, D., Reboredo, A., Lojo-Seoane, C., 2014. Do the Cambridge Neuropsychological Test Automated Battery episodic memory measures discriminate amnestic mild cognitive impairment? Int. J. Geriatr. Psychiatry 29, 602–609.

Junkkila, J., Oja, S., Laine, M., Karrasch, M., 2012. Applicability of the CANTAB-PAL computerized memory test in identifying amnestic mild cognitive impairment and Alzheimer's disease. Dement. Geriatr. Cogn. Disord. 34, 83–89.

Karperien, A., Ahammer, H., Jelinek, H.F., 2013. Quantitating the subtleties of microglial morphology with fractal analysis. Front Cell Neurosci. 7, 3.

Kettenmann, H., Kirchhoff, F., Verkhratsky, A., 2013. Microglia: new roles for the synaptic stripper. Neuron 77, 10–18.

Langston, R.F., Stevenson, C.H., Wilson, C.L., Saunders, I., Wood, E.R., 2010. The role of hippocampal subregions in memory for stimulus associations. Behav. Brain Res. 215, 275–291.
Lee, A., Archer, J., Wong, C.K., Chen, S.H., Qiu, A., 2013. Age-related decline in associative learning in healthy Chinese adults. PLoS One 8, e80648.
Liang, K.J., Lee, J.E., Wang, Y.D., Ma, W., Fontainhas, A.M., Fariss, R.N., Wong, W.T., 2009. Regulation of dynamic behavior of retinal microglia by CX3CR1 signaling. Invest. Ophthalmol. Vis. Sci. 50, 4444–4451.
Lim, S.H., Park, E., You, B., Jung, Y., Park, A.R., Park, S.G., Lee, J.R., 2013. Neuronal synapse formation induced by microglia and interleukin 10. PLoS One 8, e81218.
Lynch Alfaro, J.W., Izar, P., Ferreira, R.G., 2014. Capuchin monkey research priorities and urgent issues. Am. J. Primatol.
Ma, S., Yang, L., Romero, R., Cui, Y., 2011. Varying coefficient model for gene–environment interaction: a non-linear look. Bioinformatics 27, 2119–2126.
Miyamoto, A., Wake, H., Moorhouse, A.J., Nabekura, J., 2013. Microglia and synapse interactions: fine tuning neural circuits and candidate molecules. Front Cell Neurosci. 7, 70.
Nagahara, A.H., Bernot, T., Tuszynski, M.H., 2010. Age-related cognitive deficits in rhesus monkeys mirror human deficits on an automated test battery. Neurobiol. Aging 31, 1020–1031.
Ohsawa, K., Kohsaka, S., 2011. Dynamic motility of microglia: Purinergic modulation of microglial movement in the normal and pathological brain. Glia.
Pan, J., Kennedy, E.H., Pickering, T., Menzel, C.R., Stone, B.W., Fragaszy, D.M., 2011. Development of maze navigation by tufted capuchins (Cebus apella). Behav. Processes 86, 206–215.
Parkhurst, C.N., Yang, G., Ninan, I., Savas, J.N., Yates, J.R., Lafaille, J.J., Hempstead, B.L., Littman, D.R., Gan, W.B., 2013. Microglia promote learning-dependent synapse formation through brain-derived neurotrophic factor. Cell 155, 1596–1609.
Potì, P., Kanngiesser, P., Saporiti, M., Amiconi, A., Bläsing, B., Call, J., 2010. Searching in the middle-Capuchins' (Cebus apella) and bonobos' (Pan paniscus) behavior during a spatial search task. J. Exp. Psychol. Anim. Behav. Process 36, 92–109.
Remondes, M., Schuman, E.M., 2002. Direct cortical input modulates plasticity and spiking in CA1 pyramidal neurons. Nature 416, 736–740.
Remondes, M., Schuman, E.M., 2003. Molecular mechanisms contributing to long-lasting synaptic plasticity at the temporoammonic-CA1 synapse. Learn. Mem. 10, 247–252.
Remondes, M., Schuman, E.M., 2004. Role for a cortical input to hippocampal area CA1 in the consolidation of a long-term memory. Nature 431, 699–703.
Resende, M.C., Tavares, M.C., Tomaz, C., 2003. Ontogenetic dissociation between habit learning and recognition memory in capuchin monkeys (Cebus apella). Neurobiol. Learn Mem. 79, 19–24.
Robbins, T.W., James, M., Owen, A.M., Sahakian, B.J., McInnes, L., Rabbitt, P., 1994. Cambridge Neuropsychological Test Automated Battery (CANTAB): a factor analytic study of a large sample of normal elderly volunteers. Dementia 5, 266–281.
Rocha, E.G., Santiago, L.F., Freire, M.A., Gomes-Leal, W., Dias, I.A., Lent, R., Houzel, J.C., Franca, J.G., Pereira Jr., A., Picanco-Diniz, C.W., 2007. Callosal axon arbors in the limb representations of the somatosensory cortex (SI) in the agouti (Dasyprocta primnolopha). J. Comp. Neurol. 500, 255–266.
Rodriguez, J.S., Zurcher, N.R., Bartlett, T.Q., Nathanielsz, P.W., Nijland, M.J., 2011. CANTAB delayed matching to sample task performance in juvenile baboons. J. Neurosci. Methods 196, 258–263.
Ross, F.M., Allan, S.M., Rothwell, N.J., Verkhratsky, A., 2003. A dual role for interleukin-1 in LTP in mouse hippocampal slices. J. Neuroimmunol. 144, 61–67.
Sanchez-Ramos, J., Cimino, C., Avila, R., Rowe, A., Chen, R., Whelan, G., Lin, X., Cao, C., Ashok, R., 2012. Pilot study of granulocyte-colony stimulating factor for treatment of Alzheimer's disease. J. Alzheimers Dis. 31, 843–855.
Saper, C.B., Sawchenko, P.E., 2003. Magic peptides, magic antibodies: guidelines for appropriate controls for immunohistochemistry. J. Comp. Neurol. 465, 161–163.
Schmidt, B., Marrone, D.F., Markus, E.J., 2012. Disambiguating the similar: The dentate gyrus and pattern separation. Behav. Brain Res. 226, 56–65.
Schneider, H., Pitossi, F., Balschun, D., Wagner, A., del Rey, A., Besedovsky, H.O., 1998. A neuromodulatory role of interleukin-1beta in the hippocampus. Proc. Natl. Acad. Sci. U S A 95, 7778–7783.
Schweitzer, L., Renehan, W.E., 1997. The use of cluster analysis for cell typing. Brain Res. Brain Res. Protoc. 1, 100–108.
Scully, D., Fedriani, R., Desouza, I.E., Murphy, K.J., Regan, C.M., 2012. Regional dissociation of paradigm-specific synapse remodeling during memory consolidation in the adult rat dentate gyrus. Neuroscience 209, 74–83.
Shu, S.Y., Ju, G., Fan, L.Z., 1988. The glucose oxidase-DAB-nickel method in peroxidase histochemistry of the nervous system. Neurosci. Lett. 85, 169–171.
Skolimowska, J., Wesierska, M., Lewandowska, M., Szymaszek, A., Szelag, E., 2011. Divergent effects of age on performance in spatial associative learning and real idiothetic memory in humans. Behav. Brain Res. 218, 87–93.
Spinelli, S., Pennanen, L., Dettling, A.C., Feldon, J., Higgins, G.A., Pryce, C.R., 2004. Performance of the marmoset monkey on computerized tasks of attention and working memory. Brain Res. Cogn. Brain Res. 19, 123–137.
Spinelli, S., Ballard, T., Feldon, J., Higgins, G.A., Pryce, C.R., 2006. Enhancing effects of nicotine and impairing effects of scopolamine on distinct aspects of performance in computerized attention and working memory tasks in marmoset monkeys. Neuropharmacology 51, 238–250.
Spinozzi, G., Lagana, T., Truppa, V., 2007. Hand use by tufted capuchins (Cebus apella) to extract a small food item from a tube: digit movements, hand preference, and performance. Am. J. Primatol. 69, 336–352.
Steele, G.E., Weller, R.E., 1995. Qualitative and quantitative features of axons projecting from caudal to rostral inferior temporal cortex of squirrel monkeys. Vis. Neurosci. 12, 701–722.
Taffe, M.A., Weed, M.R., Gutierrez, T., Davis, S.A., Gold, L.H., 2002. Differential muscarinic and NMDA contributions to visuo-spatial paired-associate learning in rhesus monkeys. Psychopharmacology (Berl) 160, 253–262.
Tavares, M.C., Tomaz, C., 2002. Working memory in capuchin monkeys (Cebus apella). Behav. Brain Res. 131, 131–137.
Tremblay, M., Stevens, B., Sierra, A., Wake, H., Bessis, A., Nimmerjahn, A., 2011. The role of microglia in the healthy brain. J. Neurosci. 31, 16064–16069.
Tremblay, M.E., Lowery, R.L., Majewska, A.K., 2010. Microglial interactions with synapses are modulated by visual experience. PLoS Biol. 8, e1000527.
VanMarle, K., Aw, J., McCrink, K., Santos, L.R., 2006. How capuchin monkeys (Cebus apella) quantify objects and substances. J. Comp. Psychol. 120, 416–426.
Von Huben, S.N., Davis, S.A., Lay, C.C., Katner, S.N., Crean, R.D., Taffe, M.A., 2006. Differential contributions of dopaminergic D1- and D2-like receptors to cognitive function in rhesus monkeys. Psychopharmacology (Berl) 188, 586–596.
Wake, H., Moorhouse, A.J., Jinno, S., Kohsaka, S., Nabekura, J., 2009. Resting microglia directly monitor the functional state of synapses in vivo and determine the fate of ischemic terminals. J. Neurosci. 29, 3974–3980.
Wake, H., Moorhouse, A.J., Miyamoto, A., Nabekura, J., 2013. Microglia: actively surveying and shaping neuronal circuit structure and function. Trends Neurosci. 36, 209–217.
Wake, H., Moorhouse, A.J., Nabekura, J., 2011. Functions of microglia in the central nervous system - beyond the immune response. Neuron Glia Biol. 7, 47–53.
Wirz, A., Riviello, M.C., 2008. Reproductive parameters of a captive colony of capuchin monkeys (*Cebus apella*) from 1984 to 2006. Primates 49, 265–270.
Witter, M.P., Amaral, D.G., 1991. Entorhinal cortex of the monkey: V. Projections to the dentate gyrus, hippocampus, and subicular complex. J. Comp. Neurol. 307, 437–459.
Witter, M.P., Van Hoesen, G.W., Amaral, D.G., 1989. Topographical organization of the entorhinal projection to the dentate gyrus of the monkey. J. Neurosci. 9, 216–228.
Wong, W.T., Wang, M., Li, W., 2011. Regulation of microglia by ionotropic glutamatergic and GABAergic neurotransmission. Neuron. Glia Biol. 7, 41–46.
Zabel, M.K., Kirsch, W.M., 2013. From development to dysfunction: microglia and the complement cascade in CNS homeostasis. Ageing Res. Rev. 12, 749–756.